Improving DCP Haze Removal Scheme by Parameter Setting and Adaptive Gamma Correction

Cheng-Hsiung Hsieh[1*], Yi-Hung Chang[2]

[1)] *Department of Computer Science and Information Science, Chaoyang University of Technology, Taichung, Taiwan*

E-mail:chhsieh@cyut.edu.tw

[2)] *Department of Computer Science and Information Science, Chaoyang University of Technology, Taichung, Taiwan*

E-mail: s10827616@ cyut.edu.tw

Abstract: Recently, single-image haze removal based on the dark channel prior (DCP), originally proposed by He et. al., has attracted much attention in the image restoration community. This dehazing algorithm, called the DCP scheme here, is well-known to have four main problems in its dehazed images: artifacts, hue distortion, color over-saturation, and halos. In this paper, an improved DCP (IDCP) is proposed to deal with the four aforementioned problems, by setting the model parameters, i.e. scaling factors and window size and smoothing factor of a guided image filter in the DCP scheme. Note that a dehazed image is generally dim and low in contrast. An adaptive gamma correction (AGC) is introduced for dehazed image enhancement. The proposed IDCP and AGC are used to create the IDCP/AGC scheme, in which the IDCP scheme performs haze removal and the AGC enhances the dehazed image. The IDCP/AGC scheme was justified through extensive experiments and compared with the DCP scheme, an optimization-based scheme, and two learning-based schemes on two datasets. The results indicated that the proposed scheme is subjectively and objectively superior to the comparison schemes.

Keywords: dark channel prior, single image haze removal, adaptive gamma correction

1. INTRODUCTION

Image haze removal by far is an active research field in the image restoration and image enhancement community. The haze mainly resulted from the adversary weather condition degrades the visual quality of an image. A hazy image is generally of low contrast and visibility, which may affects the following computer visionary applications, such as video-based surveillance systems, automatic driver's assistance systems, and object tracking/recognition systems. Since haze removal is in great need, much work has been done in this field. A popular class of haze removal schemes relies on statistical observations and thus assumptions, such as contrast assumption [1], un-correlation assumption [2], dark channel prior [3], and color line [4]. Besides, in [5], a pioneer work based on machine learning for single image haze removal was proposed. In [6], a multi-scale convolutional neural networks was presented to estimate parameters in the haze image model. In [7], an end-to-end framework based on a deep learning neural network for single image haze removal was introduced. In [8], another end-to-end framework, called all-in-one dehazing network, was proposed. In [9-10], generative adversarial networks were applied to image haze removal. For more other schemes, one may consult survey papers in [11-13].

This paper will concentrate on the popular scheme based on dark channel prior, which was originated by He et al. in [3]. The scheme will be called the DCP scheme hereafter. With its

---

[*] Corresponding author: chhsieh@cyut.edu.tw

simplicity, the DCP scheme has attracted much attention recently. However, the original DCP scheme has several problems needed to be improved, i.e. computational cost, artifacts, color distortion, and halos. To reduce the computational cost, in [14] He et al. used a guided image filter (GIF) to replace the soft matting algorithm in [3] for transmission map refinement. The artifacts and color distortion usually occur in the sky region of a dehazed image, while the problem of halos happens in large depth discontinuities. To improve the DCP scheme, many researchers have proposed a variety of solutions to relieve the aforementioned problems. Some of them are listed below. In [15], with a soft segmentation, the transmission map estimation was divided into two part: one for the sky region and the other for the non-sky region. For the sky region, a luminance model was applied to estimate the transmission map, while the dark channel prior was used to estimate the transmission map in the non-sky region. Then the two transmission maps were fused to obtain the final transmission map. In [16], a sky segmentation scheme based on quad-tree splitting was presented to deal with the problem of the DCP scheme in the sky region, where the transmission map was refined by an edge preserving GIF. In [17], the sky region is segmented through a quad-tree decomposition and region-growing scheme. Then the estimate of transmission map obtained from the dark channel was modified based on the segmented sky region. The atmospheric light was estimated through the segmented sky region. In [18], the transmission map was found through minimization of an energy function with a piecewise smooth assumption. In [19], a segmentation scheme based on the binary image from gradient image of input image was employed to separate sky regions, through which an estimate of atmospheric light was found. With the help of edge information, an initial transmission map was obtained and then refined by a GIF. In [20], a light intensity reverse algorithm was proposed to deal with the artifact problem in the sky region or white objects. By a threshold, the region of interest was segmented, whose RGB pixel values were replaced with a constant manually specified by the user. Then the DCP scheme was applied to find the dehazed image. In [21], the initial transmission map was found by the 5×5 minimum filter and then refined by the Sobel filter and mean filter. To avoid color distortion, a pixel-based adaptive lower bound for the final transmission map was calculated through a constrained piece-wise linear function. In [22], a saliency detection was proposed to extract white objects according to superpixel intensity contrast. Then the atmospheric light and transmission map were estimated with the preprocessed image. Besides, an adaptive upper bound was given to avoid over-exposure in dehazed images. In [23], a two-stage transmission map estimation was employed. In the first stage, a dehazed image was found by the DCP scheme. In the second stage, the pixel-based transmission map was obtained from the dehazed image. Then morphological operations were applied to find the final transmission map. Finally, the image was restored by the final transmission map and atmospheric light estimated by the DCP scheme in the first stage.

In the aforementioned schemes, most of them use a segmentation skill to separate sky and non-sky regions to avoid the artifacts and color distortion found in the sky region, since many researchers conjecture that the problem is due to the inappropriateness of dark channel prior for the sky region. Moreover, many researchers attribute the halo problem to the large depth discontinuities in the input image. However, the two conjectures are arguable. Though the dark channel prior is not suitable in the sky region or white objects, it may not suggest that the DCP scheme is inappropriate accordingly. In [3], it says that the sky and non-sky regions can be handled gracefully, even the DCP is not a good prior for sky regions. This paper will justify that the statement is correct, through the proposed improved DCP (IDCP) scheme, where no segmentation is required for the sky and non-sky regions. In addition, problems of artifacts, hue distortion, color over-saturation, and halos in the DCP scheme will be relieved by the proposed IDCP scheme through model parameter setting. Section 3 will have the details.

In general, a dehazed image is dim and of low contrast. Conventional image enhancement methods, such as histogram equalization (HE) and gamma correction (GC), are not suitable for dehazed image enhancement, since over enhancement and color distortion happen most of

time. Even so, some researchers have tried to apply HE and GC to image haze removal. In [24], an adaptive GC was applied in the transmission map estimation. In [25], the haze image model and a GC were combined to form a model, called concise gamma-correction-based dehazing model. In their results, color distortion can be found in the given examples. In [26], a contrast limited adaptive HE (CLAHE) was applied to visibility enhancement of the dehazed image. However, over enhancement is found, when sky region is large. This paper will propose an adaptive gamma correction, which can be applied to dehazed image enhancement without color distortion.

This paper has four main contributions. First, an alternative solution is proposed to the problems of artifact and color distortion in sky regions, that is, by an adaptive scaling factor in the atmospheric light estimation. This is different from the sky and non-sky region segmentation schemes as described previously. Second, artifacts in the sky region and color distortion in a dehazed image is relieved by an adaptive scaling factor in the estimation of initial transmission map. Thus, no sky and non-sky region segmentation is required. This provides a way to mitigate this problem. Third, the halo problem happened in large discontinuities is solved by a GIF parameter setting in the transmission refinement. This doing gives a solution to the halo problem. Fourth, an adaptive gamma correction (AGC) is presented to alleviate the color distortion in the conventional gamma correction. Then the proposed AGC is employed to dehazed image enhancement. This brings for the possibility to apply gamma correction in the image haze removal field.

This paper consists of two parts. The first part is to present an improved DCP (IDCP) dehazing scheme and the second part is to introduce an adaptive gamma correction (AGC) as a post-processing to enhance the dehazed image. In Section 2, the DCP scheme is briefly reviewed. In Section 3, the proposed IDCP dehazing scheme and the proposed AGC for dehazed image enhancement are introduced. Then the two schemes are combined as the IDCP/AGC scheme. Next, the proposed IDCP/AGC scheme is extensively justified by two image datasets and compared with four dehazing schemes in Section 4. Finally, conclusion is made in Section 5.

2. REVIEW OF THE DCP SCHEME

The DCP scheme is based on the following haze image model,
$$I(x) = J(x)t(x) + A[1 - t(x)] \qquad (2.1)$$
where $I(x)$ is the observed hazy image; $J(x)$ is the haze-free image; A is the global atmospheric light or simply atmospheric light; $t(x) = e^{-\beta d(x)}$ is the transmission map which represents the portion of the non-scattered light to the camera; β is the scattering coefficient of the atmosphere and $d(x)$ is the scene depth at position x.

The DCP scheme is based on the following observation. In general, at least one of RGB components has very low intensity in the non-sky pixels of a haze-free image. This statistical observation is called dark channel prior in [3], which can be obtained through a block minimum filter. The result is called dark channel. Fig. 2.1 is an example to justify the dark channel prior where the 15×15 minimum filter is employed.

(a) (b)

Fig. 2.1. Image Forest (a) original (b) the corresponding dark channel

The derivation to obtain the initial transmission map in [3] is briefly reviewed in the following. Assume a hazy image I is in the RGB color space and without sky regions or white objects. When considering one component of I, Eq. (2.1) can be rewritten as

$$I_c(x) = J_c(x)t(x) + A_c - A_ct(x) \tag{2.2}$$

where $c \in \{R, G, B\}$. Next, Eq. (2.1) is normalized by A_c and is obtained as

$$\frac{I_c(x)}{A_c} = \frac{J_c(x)}{A_c}t(x) + 1 - t(x) \tag{2.3}$$

Assume the transmission map within the block $\Omega(x)$ is a constant. Through a block minimum filter, the dark channel in Eq. (2.3) is obtained as

$$\min_{y \in \Omega(x)} \min_c \left[\frac{I_c(x)}{A_c}\right] = \tilde{t}(x) \min_{y \in \Omega(x)} \min_c \left[\frac{J_c(x)}{A_c}\right] + 1 - \tilde{t}(x) \tag{2.4}$$

where $\tilde{t}(x)$ denotes as the initial transmission map. By the property of dark channel prior, the dark channel for haze-free image $J_c(x)$ approaches to zero and thus $\min_{y \in \Omega(x)} \min_c \left[\frac{J_c(x)}{A_c}\right] = 0$ is considered in Eq. (2.4). Consequently, by Eq. (2.4) the initial transmission map can be estimated from the input image I as

$$\tilde{t}(x) = 1 - \min_{y \in \Omega(x)} \min_c \left[\frac{I_c(x)}{A_c}\right] \tag{2.5}$$

To avoid the halo problem, the initial transmission map $\tilde{t}(x)$ is further refined by the soft matting algorithm in [3] or a guided image filter (GIF) in [14]. For more details, one may consult [3, 14].

Given image I in the RGB color space, the implementation steps of the DCP scheme are given as follows.

Step 1. Find the initial block dark channel through a block minimum filter as

$$I_\Omega^{dark}(x) = \min_{y \in \Omega(x)} \min_c [I_c(y)] \tag{2.6}$$

where $\Omega(x)$ is a $N \times N$ window centered at x and $c \in \{R, G, B\}$. In [3], $N = 15$ is employed.

Step 2. Estimate the atmospheric light $A = [A_R \ A_G \ A_B]$ by $I_\Omega^{dark}(x)$. Find the 0.1% pixels of the highest values in $I_\Omega^{dark}(x)$; trace back to the corresponding pixels in image I; and find the pixel with the highest intensity as the estimate of A.

Step 3. Calculate the normalized block dark channel as

$$\bar{I}_\Omega^{dark}(x) = \min_{y \in \Omega(x)} \min_c \left[\frac{I_c(y)}{A_c}\right] \tag{2.7}$$

Step 4. Obtain the initial transmission map as

$$\tilde{t}(x) = 1 - \omega \times \bar{I}_\Omega^{dark}(x) \tag{2.8}$$

where $0 < \omega \leq 1$ is a scaling factor. In [3], ω is set to 0.95.

Step 5. Refine the initial transmission map $\tilde{t}(x)$ by the soft matting algorithm in [3] or by the GIF) in [14] to obtain the final transmission map $t(x)$. When the GIF is used, the settings given in [14] are as follows: the input image I as the guidance image; the window size $N = 20$; the smoothing factor $\epsilon = 0.001$.

Step 6. Recover the scene radiance as

$$\hat{J}_c(x) = \frac{I_c(x) - A_c}{\max[t_0, t(x)]} + A_c \tag{2.9}$$

where t_0 is a user-defined lower bound of $t(x)$. It is set to 0.1 in [3].

3. THE PROPOSED IDCP SCHEME AND AGC

This section will introduce the proposed IDCP haze removal scheme and the AGC for dehazed image enhancement in this study. In Section 3.1, the IDCP scheme is presented to improve the DCP performance. Then, the post-processing AGC scheme is proposed to enhance the visual quality of the dehazed image by the IDCP scheme in Section 3.2.

3.1. The IDCP dehazing scheme

It is well-known that for better performance, at least four problems should be appropriately addressed in the DCP scheme: estimation of A, estimation of $t(x)$, the sky/non-sky region handling, and halos. The solutions in the IDCP scheme are given below.

3.1.1. Atmospheric light estimation

In the DCP scheme, the hue distortion is often found in the dehazed images, especially in the sky region. To see the problem, image Village is served as an example, which is shown in Fig. 3.1(a). The dehazed image by the DCP is shown in Fig. 3.1(b) where the sky region is of hue distortion. In [27], it has proven that the hue distortion in a dehazed image results from the estimation error of A. In other words, the problem of hue distortion in the DCP scheme is from an inappropriate estimation of A. Fortunately, the problem can be relieved by introducing a scaling factor α on A. In the DCP scheme, the scaling factor of A can be considered as $\alpha = 1$ as in Eq. (2.6). When $\alpha = 0.85$, the dehazed image is shown in Fig. 3.1(c). Obviously, the hue distortion is relieved by scaling α value. Thus, an adaptive scaling factor α_a will be employed in the IDCP scheme. By experiments, $\alpha_a = \min[(\mu_1)^{0.0975}, 0.975]$ works well most of time, where $\mu_1 = \text{mean}[I_1^{dark}(x)]$ and I_1^{dark} the pixel-based dark channel. Besides, $I_\Omega^{dark}(x)$ in Step 2 of the DCP scheme is replaced by I_1^{dark} to find A for efficiency.

(a)   (b)   (c)

Fig. 3.1. Image Village (a) original (b) $\alpha = 1$ (c) $\alpha = 0.85$

3.1.2. Initial transmission map estimation

In the DCP scheme, the fixed scaling factor $\omega = 0.95$, as in Eq. (2.8), is used to find the initial transmission map $\tilde{t}(x)$ according to the aerial perspective phenomenon. However, we find that artifacts in the sky region and color distortion in a dehazed image are caused by the inappropriate fixed scaling factor $\omega = 0.95$. Thus, it introduces the related distortions accordingly. To see the problem, image Dogs is given as an example, which is shown in Fig. 3.2(a). After the DCP scheme, the dehazed image is depicted in Fig. 3.2(b), which shows the artificial contours and color distortion due to $\omega = 0.95$. Fortunately, an adaptive scaling factor ω_a can help the situation. With $\omega = 0.65$, the result is given in Fig. 3.2(c). In the IDCP scheme, an adaptive scaling factor ω_a will be employed to estimate initial transmission map $\tilde{t}(x)$. As a rule of thumb, $\omega_a = \min[(\mu_{0.9})^{0.325}, 0.95]$ is employed where $\mu_{0.9} = \text{mean}[\bar{I}_\Omega^{dark}(x) \leq 0.9]$ and $\bar{I}_\Omega^{dark}(x)$ the normalized block-based dark channel.
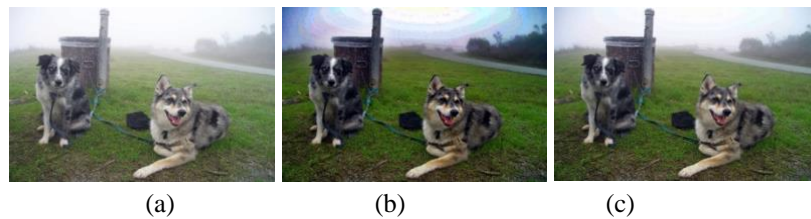

(a)   (b)   (c)

Fig. 3.2. Image Dogs (a) original (b) $\omega = 0.95$ (c) $\omega = 0.65$

3.1.3. Sky and non-sky region handling

In [3], it says that the sky and non-sky regions can be handled gracefully, even the DCP is not a good prior for sky regions. The statement can be verified as follows. In a bright sky region, the pixel intensity $I_c(x) \to 1$; the atmospheric light $A_c \to 1$; the normalized dark channel $\bar{I}_\Omega^{dark}(x) \to 1$; the transmission map $t(x) \to 1$, and thus the dehazed scene can be found as

$$\hat{J}_c(x) = \frac{I_c(x) - A_c}{\max[t_0, t(x)]} + A_c \to A_c \qquad (3.1)$$

which is generally consistent with the real situation. Consequently, by Eq. (3.1) there is no need to handle sky and non-sky regions separately, though many published papers headed

toward the way to the sky/non-sky region segmentation. In other words, the DCP scheme can be applied to the sky and non-sky regions equally well, if appropriate parameters are employed. By our observations, the problems of color over-saturation distortion, hue distortion, artifacts, and over-exposure found in the sky region come from inappropriate estimations of A and $t(x)$. This can be verified by Fig. 3.1 and Fig. 3.2. In the IDCP scheme, these problems can be relieved by setting parameters appropriately.

3.1.4. Initial transmission map refinement

In general, halos occur in the large depth discontinuities of a dehazed image. It is observed that the halo problem in the DCP scheme comes from an inappropriate parameter setting in the GIF for transmission map refinement. In the GIF, three parameters are guidance image I_g, window size N, and smoothing factor ϵ. In the DCP scheme, I_g is the input image I; $N = 20$; $\epsilon = 0.001$. By observations, we find that appropriately setting parameters N and ϵ in the GIF is able to deal with the halo problem. A large N in the GIF reduces the halo effect in a dehazed image. However, it introduces minor color over-saturation. Fortunately, it can be solved by using a large ϵ.

A. The effect of N

Here, image House, shown in Table 3.1, is used as an example to investigate the effect of the GIF parameters, N and ϵ, on a dehazed image. In the simulation, the DCP scheme is employed with the GIF setting $N = 20$ and $\epsilon = 0.001$, as suggested in [14]. To investigate the effect of parameter N, ϵ is fixed at 0.001. The dehazed images with different values of N, i.e. 20, 40, and 55, are given in Table 3.1, where the corresponding refined transmission $t(x)$ are also shown for comparison. In the case of $N = 20$, the dehazed House has a severe halo problem at large depth discontinuities. As N increases to 40, the halos diminish significantly. When $N = 55$, the halo is not visible at all. Besides, one may observe that the significant edges in $t(x)$ become more clear and more details appear, as N varies from 20 to 55. It implies that a large window size may avoid the halo problem, as expected. Consequently, $N = 55$ will be used in the proposed IDCP scheme. Though the window size $N = 55$ is able to deal with the halo problem, minor color over-saturation is found in the dehazed House, as shown in the fourth row of Table 3.1. Fortunately, the introduced distortion can be avoided by setting smoothing factor ϵ. The following subsection has the details.

Table 3.1. The effect of N in the GIF on the dehazed image House.

GIF setting	$t(x)$	$\hat{J}(x)$	Original image
$N = 20$ $\epsilon = 0.001$			
$N = 40$ $\epsilon = 0.001$			
$N = 55$ $\epsilon = 0.001$			

B. The effect of ϵ

The effect of smoothing parameter ϵ on the dehazed House is investigated here. In the simulation, ϵ is set to 0.001, 0.05, and 0.1, where N is fixed at 55. The corresponding dehazed images and their corresponding $t(x)$ are given in Table 3.2, respectively. By Table 3.2, one can observe that the details of $t(x)$ has been smoothened more and more, as ϵ increases from 0.001 to 0.1. Besides, the problem of color over-saturation gradually relieves, as ϵ becomes larger. It suggests that the problem of color over-saturation can be dealt with a large ϵ, i.e. 0.1. Thus, the smoothing factor $\epsilon = 0.1$ will be employed in the proposed IDCP scheme.

Table 3.2. The effect of ϵ in the GIF on the dehazed image House.

GIF setting	$t(x)$	$\hat{J}(x)$	Original image
$N = 55$ $\epsilon = 0.001$			
$N = 55$ $\epsilon = 0.05$			
$N = 55$ $\epsilon = 0.1$			

3.1.5. Implementation of the IDCP scheme

With the above discussion, the proposed IDCP scheme is summarized in the following implementation steps, where input image I is assumed in the RGB color space.

Step 1. Find the pixel-based dark channel as

$$I_1^{dark}(x) = \min_c [I_c(x)] \tag{3.2}$$

where $c \in \{R, G, B\}$.

Step 2. Find the maximum in $I_1^{dark}(x)$ and its corresponding pixel in I, p_{max}. Then estimate the atmospheric light as $A = [A_R \ A_G \ A_B] = \alpha_a \times p_{max}$, where $\alpha_a = \min[(\mu_1)^{0.0975}, 0.975]$ and $\mu_1 = \text{mean}[I_1^{dark}(x)]$.

Step 3. Calculate the normalized block-based dark channel as

$$\bar{I}_\Omega^{dark}(x) = \min_{y \in \Omega(x)} \min_c \left[\frac{I_c(y)}{A_c}\right] \tag{3.3}$$

Step 4. Obtain the initial transmission map as

$$\tilde{t}(x) = 1 - \omega_a \times \bar{I}_\Omega^{dark}(x) \tag{3.4}$$

where $\omega_a = \min[(\mu_{0.9})^{0.325}, 0.95]$ and $\mu_{0.9} = \text{mean}[\bar{I}_\Omega^{dark}(x) \leq 0.9]$.

Step 5. Find the final transmission map $t(x)$ through refining $\tilde{t}(x)$ by the GIF with the guidance image $I_1^{dark}(x)$, the window size $N = 55$, and the smoothing parameter $\epsilon = 0.1$.

Step 6. Estimate the dehazed image as

$$\hat{J}_c(x) = \frac{I_c(x) - A_c}{\max[t_0, t(x)]} + A_c \tag{3.5}$$

where $t_0 = 0.1$ is a user-defined lower bound of $t(x)$.

In comparison with the DCP scheme described in Section 2, the proposed IDCP scheme has at least four main differences. First, the pixel-based dark channel $I_1^{dark}(x)$ is used to estimate the atmospheric light $\boldsymbol{A}$ with an adaptive scaling factor α_a. Second, $I_1^{dark}(x)$ is employed as the guidance image in the GIF to refine the initial transmission map $\tilde{t}(x)$. This helps improve the efficiency. Third, an adaptive scaling factor ω_a is applied in the estimation of initial transmission map $\tilde{t}(x)$ to avoid the artifacts and color distortion happened in the sky region. This doing makes the proposed IDCP scheme is able to deal with the sky and non-sky regions equally well, without segmentation. Fourth, the GIF setting with large $N = 55$ is employed to relieve the halo problem, while large $\epsilon = 0.1$ is to handle the color over-saturation. With those modifications, the proposed IDCP scheme shows much better performance than the DCP scheme. This will be verified in Section 4.

3.2. Dehazed Image Enhancement with an AGC

A dehazed image generally is dimmer than its original image. Consequently, an adaptive gamma correction (AGC) is used to improve visual quality of dehazed images. The AGC is modified from a conventional gamma correction (CGC). Given image $\boldsymbol{I}_i$, whose elements are denoted as $I_i^c(x)$ and $c \in \{R, G, B\}$, a CGC transforms $I_i^c(x)$ to a new value $I_o^c(x)$ as

$$I_o^c(x) = \left[\frac{I_i^c(x)}{I_H^c}\right]^g I_H^c \tag{3.6}$$

where $I_H^c = \max_x[I_i^c(x)]$ is the maximum value in component c. When put the dynamic ranges of input image $\boldsymbol{I}_i$ and output image $\boldsymbol{I}_o$ into account, Eq. (3.6) can be rewritten in a more general form as

$$I_o^c(x) = \left[\frac{I_i^c(x)-I_L^c}{I_H^c-I_L^c}\right]^g \left[I_{o,H}^c - I_{o,L}^c\right] + I_{o,L}^c \tag{3.7}$$

where $I_L^c = \min_x[I_i^c(x)]$ and $I_H^c = \max_x[I_i^c(x)]$. Notations $I_{o,L}^c$ and $I_{o,H}^c$ are user-defined lower limit and upper limit of $I_o^c(x)$ for the output image $\boldsymbol{I}_o$, respectively. The superscript g in Eq. (3.7) is a user-defined factor. It is well-known that the CGC suffers from the problem of color distortion. Therefore, it hinders the application to dehazed image enhancement. An example, image Women, is given in Fig. 3.3(a), where the dehazed image, shown in Fig. 3.3(b), is obtained by the proposed IDCP scheme. The dehazed image, post-processed by the CGC, is shown in Fig. 3.3(c) which has a noticeable color distortion.

| (a) | (b) | (c) | (d) |

Fig. 3.3. Image Women (a) original (b) after the proposed IDCP scheme (c) with the CGC (d) with the AGC

To relieve the color distortion in the CGC, an adaptive gamma correction (AGC) is introduced here. By our observations, the color distortion in the CGC results from the inappropriate set of upper and lower limits, $[I_L^c \ I_H^c]$. Consequently, the proposed AGC replaces the set $[I_L^c \ I_H^c]$ with set $[I_L \ I_H]$ where $I_L = \min_c[I_L^c]$ and $I_H = \max_c[I_H^c]$. With the set $[I_L \ I_H]$, Eq. (3.7) is modified as

$$I_o^c(x) = \left[\frac{I_i^c(x)-I_L^c}{I_H-I_L}\right]^{g_a} \left[I_{o,H}^c - I_{o,L}^c\right] + I_{o,L}^c \tag{3.8}$$

where g_a is an adaptive factor.

The way to determine parameter g_a in Eq. (3.8) is discussed below. Note that the parameter ω_a for initial transmission map estimation affects the strength of haze removal significantly. That is, a larger ω_a results in a stronger dehazing effect and vice versa. A stronger haze removal makes the dehazed image dimmer in general. Consequently, g_a should be inversely

related to ω_a. To increase the brightness, g_a is restricted to be less than 1 and greater than 0.7 to avoid artifacts. By experiments, $g_a = \max[(1 - \omega_a)^{0.095}, 0.707]$ is employed in the AGC. With this g_a, the proposed AGC is applied to Fig. 3.3(b), whose result is shown in Fig. 3.3(d). As expected, the color distortion is avoided and visual quality is enhanced. Since the proposed AGC is a post-processing scheme, it can be added to the proposed IDCP scheme after Step 6 in Section 3.1.5. That is,

Step 7.   Enhance the dehazed image $\hat{J}$ by the AGC.

The combination of the IDCP scheme and the AGC will be call the IDCP/AGC scheme.

4. RESULTS AND DISCUSSIONS

In this section, the proposed IDCP/AGC scheme is justified by the datasets RESIDE in [13] and KeDeMa in [28]. The RESIDE dataset is a large-scale benchmark for single image dehazing algorithms, which consists of synthetic and natural images. In the following experiments, the indoor training set (ITS) [29] is employed, that has 10,000 clear images and 100,000 synthetic hazy images generated by Eq. (2.1) with various A and β. Besides, the outdoor training set (OTS) [30] is also used, which consists of 3,981 clear images and 136,160 synthetically generated hazy images. By the large amount of images, the proposed IDCP/AGC scheme is justified and compared with four recently reported haze removal schemes in Section 4.1, where both objective and subjective evaluation are considered. The four compared schemes are the conventional DCP scheme in [14], the optimization-based scheme in [31], which will be called RRO scheme, the learning based scheme in [32], which will be called CAP scheme, and the deep learning based scheme DehazeNet (DNet for short) in [33]. In Section 4.2, the KeDeMa dataset is used, which consists of 25 natural hazy images with different scenarios, to further verify for the proposed IDCP/AGC scheme, objectively and subjectively, and compared with the DCP, RRO, CAP, and DNet schemes.

In addition to the subjective comparison, the performances of the related schemes are also justified objectively. To compare the related schemes in different aspects, the objective assessments include full-reference methods: the peak signal-to-noise ratio (PSNR) and the structural similarity index measure (SSIM) in [34]; half-reference method: the dehazing quality index (DHQI) in [35]; no-reference methods: the blind/reference-less image spatial quality evaluator (BRISQUE) in [36] and the integrated local natural image quality evaluator (IL-NIQE) in [37]. The compared results are given below.

4.1 Results and comparisons with the RESIDE dataset

To justify the performance of the proposed IDCP/AGC scheme, an extensive experiment is conducted with the RESIDE dataset in this section, where the results from the four compared schemes are also given for objective and subjective comparisons. First, the proposed IDCP/AGC scheme and the compared schemes are run with the ITS dataset in Section 4.1.1 and then OTS dataset in Section 4.1.2.

4.1.1. Results with the ITS dataset

In this subsection, the IDCP/AGC scheme is verified by the ITS dataset. The results for the four compared schemes are also given for comparison. The first part shows the objective results, where the performance indices PSNR, SSIM, DHQI are better for a higher value, while BRISQUE, IL-NIQE are the less the better. In the second part, subjective results will give for visual comparison.

A. Objective comparison with the ITS dataset

The objective comparisons with PSNR, SSIM, DHQI, BRISQUE, IL-NIQE are shown in Table 4.1, for the proposed IDCP/AGC scheme and the compared schemes, where the ranking is shown in parentheses. By the results, the DCP scheme has the best and second best in

BRISQUE and IL-NIQE, respectively. However, it has the worst ranking in PSNR, SSIM, and DHQI. That is, the DCP scheme lies on either the worst end or the best end with the average ranking 3.6. For the RRO scheme, it ranks the second best in BRISQUE; the third place in DHQI and IL-NIQE; the fourth place in PSNR and SSIM. It ends with the average ranking 3.2. As for the CAP scheme, it has the second best PSNR; the third place in SSIM; but the fourth place in DHQI and BRISQUE, and the worst ranking in IL-NIQE. The average ranking is 3.6. As for the DNet, it has the best PSNR and SSIM; the second best in DHQI; but the fourth place in IL-NIQE and the worst ranking in BRISQUE. Its average ranking is 2.6. The ranking of the proposed IDCP/AGC scheme falls within the top three among full-reference, semi-reference, and no-reference assessments. It suggests that the performance of the proposed IDCP/AGC scheme has a relatively stable performance among the compared schemes. Overall, the proposed IDCP/AGC scheme has the best performance, then DNet, RRO, CAP, and DCP schemes, in terms of the average ranking (AR).

Table 4.1. Objective comparison with the ITS dataset

	IDCP/AGC	DCP	RRO	CAP	DNet
PSNR	19.1669(3)	16.4216(5)	18.2363(4)	19.5537(2)	20.3097(1)
SSIM	0.8742(2)	0.8374(5)	0.84681(4)	0.8733(3)	0.8909(1)
DHQI	59.8120(1)	55.6912(5)	57.3045(3)	56.9135(4)	59.2964(2)
BRISQUE	15.6748(3)	13.4386(1)	13.9044(2)	19.1409(4)	22.6275(5)
IL-NIQE	32.6799(1)	33.4390(2)	33.5820(3)	33.9286(5)	35.3254(4)
AR	2(1)	3.6(4)	3.2(3)	3.6(4)	2.6(2)

B. Subjective comparison with the ITS dataset

In addition of objective comparison, the subjective comparison is also given for the ITS dataset. Here, six images are selected to subjectively evaluate the proposed IDCP/AGC scheme and the compared schemes. The six images include two less hazy images (No. 1 and No. 2), two moderate hazy images (No. 3 and No. 4), and two heavy hazy images (No. 5 and No. 6), which are shown in Table 4.2. For reference, the image filenames in ITS are also given in Table 4.2 with the associated PSNR for each selected image. By Table 4.2, the DCP scheme tends to have hue distortion and color over-saturation in all six dehazed images. The RRO scheme has hue distortion in images 2, 4, and 5; minor color over-saturation for images 1 and 3. The dehazing effect of the CAP scheme seems not strong enough, especially for the heavy hazy images 5 and 6. Basically, the DNet scheme performs well in the cases of less hazy and moderate images, but fails to remove haze in heavy hazy images 5 and 6. As for the proposed IDCP/AGC scheme, it provides better visual quality in the dehazed images.

Table 4.2. Subjective comparison with the ITS dataset (6 selected images)

No	Clear	Input	IDCP/AGC	DCP	RRO	CAP	DNet
1							
		0025_08_0.7048	PSNR=31.26	16.32	24.97	22.42	20.17
2							
		1075_03_0.7312	PSNR=30.72	13.29	13.96	24.53	25.63
3							
		0499_05_0.8353	PSNR=22.63	15.50	21.89	19.78	21.47

No	Clear	Input	IDCP/AGC	DCP	RRO	CAP	DNet
4							
		0691_09_0.8315	PSNR=24.53	19.06	18.08	20.01	23.91
5							
		0803_10_0.9055	PSNR=22.97	13.28	13.83	19.42	19.44
6							
		0962_02_0.7819	PSNR=22.56	18.43	15.69	14.01	14.77

Next, three worse cases, shown in Table 4.3, for the proposed IDCP/AGC scheme are given and discussed. For image 1, better visual quality is for the proposed IDCP/AGC scheme, even though the CAP and DNet schemes have better PSNR. It suggests that the PSNR is not consistent with the subjective evaluation in some cases. Similar results are found in images 2 and 3. The dehazed images by the proposed IDCP/AGC scheme are obviously better than the compared schemes, even some of their PSNR are higher. The reason might be that the proposed IDCP/AGC scheme enhances the contrast and brightness in the dehazed images. Thus, it increases the mean squared error between the dehazed images and their clear images, and lower PSNR results. Consequently, in this study five objective assessments are employed to have a more fair comparison among the proposed IDCP/AGC scheme and the compared schemes.

Table 4.3. Subjective comparison with the ITS dataset (3 chosen cases)

No	Clear	Input	IDCP/AGC	DCP	RRO	CAP	DNet
1							
		0244_02_0.8649	PSNR=25.28	16.14	15.09	33.10	34.54
2							
		0388_09_0.7129	PSNR=20.84	16.78	30.50	25.11	29.11
3							
		0146_04_0.7433	PSNR=15.72	16.07	27.77	24.16	21.88

4.1.2. Results with the OTS dataset

To have more understanding the performance, the proposed IMDCP/AGLGC scheme is further justified by the OTS dataset and compared with the DCP, RRO, CAP, and DNet schemes. The objective comparison is given first and then the subjective comparison follows.

A. Objective comparison with the OTS dataset

As in the ITS dataset, five objective assessments, PSNR, SSIM, DHQI, BRISQUE, and IL-NIQE, for the proposed IDCP/AGC scheme, DCP, RRO, CAP, and DNet are given in Table 4.4. The DCP scheme has the second best in IL-NIQE and the third place in BRISQUE, but with the worst PSNR, SSIM, and DHQI. This ends up with average ranking 4. For the RRO scheme, it has the second best in BRISQUE, the third place in IL-NIQE, and the fourth place in PSNR, SSIM, and DHQI. Its average ranking is 3.4. The CAP scheme has the best SSIM and the second best PSNR, the third place DHQI, but the fourth place in BRISQUE and IL-NIQE, which results in the average ranking 2.8. For the DNet, it has the best PSNR and DHQI, the second best in SSIM, but the worst BRISQUE and IL-NIQE. The average ranking is 2.8. As for the proposed IDCP/AGC scheme, it has the best BRISQUE and IL-NIQE, the second best DHQI, and the third place in PSNR and SSIM. Its average ranking is 2. By the average

ranking, the best one is the proposed IDCP/AGC scheme, and then DNet or CAP, RRO, and DCP at final. By Table 4.4, it implies that the proposed IDCP/AGC scheme has more stable performance than the compared schemes, among the five objective assessments.

Table 4.4. Objective comparison with the OTS dataset

	IDCP/AGC	DCP	RRO	CAP	DNet
PSNR	22.5973(3)	15.9340(5)	19.0970(4)	23.3067(2)	23.7265(1)
SSIM	0.9111(3)	0.8456(5)	0.8779(4)	0.9236(1)	0.9161(2)
DHQI	50.6845(2)	44.9371(5)	47.7001(4)	49.9232(3)	51.6284(1)
BRISQUE	16.1972(1)	16.9098(3)	16.3732(2)	16.9410(4)	19.0443(5)
IL-NIQE	21.2804(1)	21.3985(2)	21.4482(3)	21.4876(4)	23.1376(5)
AR	2(1)	4(4)	3.4(3)	2.8(2)	2.8(2)

B. Subjective comparison with the OTS dataset

For subjective comparison, six images are selected from the OTS dataset, which are shown in Table 4.5. The six images are with different haziness. Two images (No. 1 and No. 2) are less hazy, two images (No. 3 and No. 4) are of moderate haziness, and two images (No. 5 and No. 6) have more haziness. The corresponding PSNR for each image is also given in Table 7 for reference. In the given images, the DCP scheme has artifacts in image 2, color over-saturation in images 3 and 4 , and hue distortion in images 5 and 6. The RRO scheme has less dehazing effect in image 1, artifacts in image 2, hue distortion in images 3 and 5, and minor color over-saturation in images 4 and 6. The CAP scheme has a dark chiffon in images 5 and 6. Similarly, the DNet scheme has similar, but minor, results in images 5 and 6. For the rest of images, the DNet generally works better than the CAP scheme, in terms of visual quality of the dehazed images. As for the proposed IDCP/AGC scheme, it gives better subjective results than the four compared schemes, even images 3, 5, and 6 have less PSNR, which is caused by brightness and contrast enhancement.

Table 4.5. Subjective comparison with the OTS dataset (6 selected images)

No	Clear	Input	IDCP/AGC	DCP	RRO	CAP	DNet
1		1178_0.8_0.04	PSNR=34.09	26.94	22.88	25.56	24.14
2		0014_1_0.04	PSNR=23.21	14.52	19.62	21.63	19.14
3		0255_1_0.1	PSNR=26.11	18.55	18.09	25.65	27.06
4		0250_0.85_0.12	PSNR=25.72	15.90	17.88	23.07	24.06
5		0027_0.8_0.2	PSNR=21.02	14.38	23.01	20.68	25.01

6							
		0004_0.8_0.2	PSNR=19.29	12.77	17.00	21.47	14.77

For the OTS dataset, three worse cases in the proposed IDCP/AGC scheme are given and discussed here. The three images are shown in Table 4.6, where their PSNR are given as well. Obviously, the visual quality of the dehazed images by the proposed IDCP/AGC scheme is better than the four compared schemes, even though some of PSNR are lower. For images 1 and 2, the ground true image, i.e. clear image, is somewhat hazy, not really clear. Thus, it affects the PSNR calculation. In other words, the schemes have less dehazing effect, like the RRO, CAP, and DehazeNet, achieve better PSNR. For image 3, it is a night shot. The proposed IDCP/AGC scheme not only removes haze but also enhances brightness and contrast. Consequently, it increases the mean squared error and thus less PSNR results. It explains why the proposed IDCP/AGC scheme takes the third place in PSNR, as shown in Table 4.6. That is why this study adopts five different objective assessments and the average ranking is used to evaluate the overall performance for a fair comparison.

Table 4.6. Subjective comparison with the OTS dataset (3 chosen cases)

No	Clear	Input	IDCP/AGC	DCP	RRO	CAP	DNet
1							
		0267_0.95_0.16	PSNR=25.10	14.97	20.02	30.58	26.96
2							
		0150_0.85_0.2	PSNR=16.36	16.38	16.69	32.36	19.74
3							
		0113_0.85_0.12	PSNR=15.94	29.45	19.40	18.13	26.31

4.2 Results and Comparisons with the KeDeMa dataset

In this section, the proposed IDCP/AGC scheme is applied to the natural images, where no ground true images are available. In the experiments, the KeDeMa dataset, which contains 25 natural hazy images, is employed to verify the proposed IDCP/AGC scheme further, whose results are compared with the DCP, RRO, CAP, and DNet schemes as previously.

4.2.1 Objective comparison with the KeDeMa dataset

Three objective metrics, DHQI, BRISQUE, and IL-NIQE, are calculated with the dehazed images obtained by the proposed IDCP/AGC and the compared schemes. Note that the full reference metrics, PSNR and SSIM, are not applicable, since ground true images are not available. For those three metrics do not require ground true images, the results are shown in Table 4.7. By Table 4.7, the DCP scheme ranks between 3 and 5; the RRO scheme lies within top three ranking; the CAP scheme takes the best in BRISQUE and the fourth place in DHQI and IL-NIQE; the DNet scheme has the worst ranking in BRISQUE and IL-NIQE, and the third place in DHQI; the proposed IDCP/AGC scheme has the best DHQI, and the second best both in BRISQUE and IL-NIQE. By the average ranking, the proposed IDCP/AGC scheme outperforms the compared schemes, and the RRO, CAP, DCP, and DNet schemes follow. Again, the proposed IDCP/AGC scheme provides a better and more stable performance than the compared schemes.

**Table 4.7.** Objective comparison with the KeDeMa dataset

	IDCP/AGC	DCP	RRO	CAP	DNet
DHQI	60.5390(1)	57.7240(5)	60.1320(2)	58.9870(4)	61.1010(3)
BRISQUE	11.8990(2)	12.5420(4)	12.3470(3)	10.9520(1)	13.3190(5)
IL-NIQE	23.9100(2)	24.6400(3)	23.5640(1)	25.6000(4)	27.7350(5)
AR	1.7(1)	4(4)	2(2)	3(3)	4.3(5)

4.2.2 Subjective comparison with the KeDeMa dataset

For subjective comparison, the 25 dehazed images for the KeDeMa dataset are shown in Table 4.8, which are obtained from the proposed IDCP/AGC scheme and the four compared schemes. In general, the DCP scheme suffers from the problems of color over-saturation, halos, and artifacts throughout the given examples. The RRO scheme has artificial contours in the sky region of image 1, hue distortion in image 5, color over-saturation in image 7, less dehazed results in images 9, 11. For the CAP scheme, it has artificial contours in the sky region of image 1, and less dehazed results in images 3 to 6, 8, 18 to 23. Generally, the CAP scheme has a relatively weak dehazing performance. The DNet scheme has artificial contours in the sky region of image 1, less dehazed results in images 3, 4, 6, 11, 18, 20, 21, 22, and 23. As for the proposed IDCP/AGC scheme, it generally gives a stable and better result than the compared schemes in visual quality, which is demonstrated in the aspects of naturalness, brightness, and contrast, as shown in Table 4.8.

Table 4.8. Subjective comparison with the KeDeMa dataset
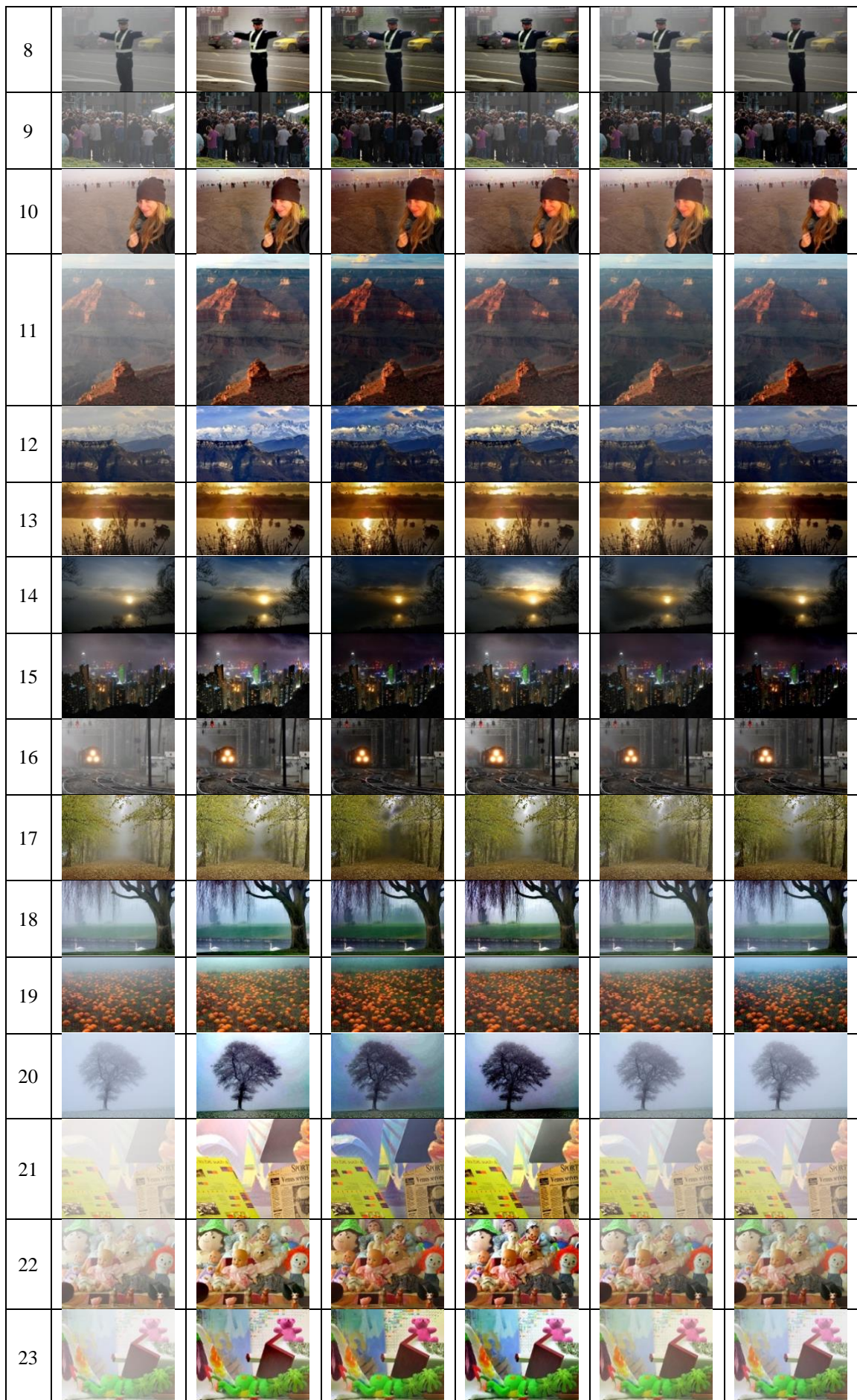
5. CONCLUSION

In this paper, an improved DCP (IDCP) scheme was presented to solve the four problems in the DCP scheme: artifacts, hue distortion, color over-saturation, and halos. The dehazed image by the IDCP was further enhanced by an adaptive gamma correction (AGC). The overall dehazing scheme is called IDCP/AGC. The proposed IDCP/AGC scheme was extensively justified by the synthetic hazy images in the ITS and OTS datasets, and the natural images in the KeDeMa dataset. Besides, the proposed IDCP/AGC scheme was compared with four recently reported haze removal schemes objectively and subjectively. To have a balanced comparison, five objective assessments, including full-reference, half-reference, and no-reference methods, were employed. The results indicated that the objective evaluation was for the proposed IDCP/AGC scheme in terms of the average ranking, while the subjective comparison showed that the proposed IDCP/AGC scheme was relatively stable and able to provide a better visual quality in the given image datasets. In the future, an optimization algorithm will be investigated for the heuristic parameter setting in the proposed IDCP/AGC scheme.

REFERENCES

1. Tan, R.T. (2008). Visibility in bad weather from a single image, Proc. of IEEE Conference on Computer Vision and Pattern Recognition, Anchorage, AK, 1-8, doi: 10.1109/CVPR.2008.4587643

2. Fattal, R. (2008). Single image dehazing, *ACM Transactions on Graphics*, 27(3), 721-729, 2008, doi: 10.1145/1360612.1360671

3. He, K., Sun, J., and Tang, X. (2011). Single image haze removal using dark channel prior, *IEEE Transactions on Pattern Analysis and Machine Intelligence*, 33(12), 2341-2353, doi: 10.1109/TPAMI.2010.168

4. Fattal, R. (2014). Dehazing using color-lines," *ACM Transactions on Graphics*, Article number: 13, doi: 10.1145/2651362

5. Zhu, Q., Mai, J., and Shao, L. (2015). A fast single image haze removal algorithm using color attenuation prior, *IEEE Transactions on Image Processing*, 24(11) 3522-3533, doi: 10.1109/TIP.2015.2446191

6. Ren, W., Liu, S., Zhang, H., Pan, J., Cao, X., et. al. (2016). Single image dehazing via multi-scale convolutional neural networks, *Proc. of Europe Conference on Computer Vision*, 154-169, 2016, doi: 10.1007/978-3-319-46475-6_10

7. Cai, B., Xu, X., Jia, K., Qing, C., and Tao, D. (2016). DehazeNet: an end-to-end system for single image haze removal, *IEEE Transactions on Image Processing*, 25(11), 5187-5198, doi: 10.1109/TIP.2016.2598681

8. Li, B., Peng, X., Wang, Z., Xu, J., and Feng, D. (2017). AOD-Net: all-in-one dehazing network, *Proc. of IEEE International Conference on Computer Vision*, Venice, 4780-4788, doi: 10.1109/ICCV.2017.511

9. Chen, Y., Patel, A.K., and Chen, C. (2019). Image haze removal by adaptive CycleGAN, *Proc. of Asia-Pacific Signal and Information Processing Association Annual Summit and Conference*, Lanzhou, China, 1122-1127, doi: 10.1109/APSIPAASC47483.2019.9023296

10. Liu, Z., Xiao, B., Alrabeiah, M., Wang, K., and Chen, J. (2019). Single image dehazing with a generic model-agnostic convolutional neural network, *IEEE Signal Processing Letters*, 26(6), 833-837, doi: 10.1109/LSP.2019.2910403

11. Lee, S., Yun, S., Nam, J.-H., Won, C.S., and Jung, S.-W. (2016). A Review on dark channel prior based image dehazing algorithms, *EURASIP Journal on Image and Video Processing*, Article number: 4, doi: 10.1186/s13640-016-0104-y

12. Singh, D., and Kumar, V. (2018). Comprehensive survey on haze removal techniques, *Multimedia Tools and Applications*, 77, 9595–9620, doi: 10.1007/s11042-017-5321-6

13. Li, B., Ren, W., Fu, D., Tao, D., Feng, D., et. al. (2019). Benchmarking single-image dehazing and beyond, *IEEE Transactions on Image Processing*, 28(1), 492-505, doi: 10.1109/TIP.2018.2867951

14. He, K., Sun, J., and Tang, X. (2013). Guided image filtering, *IEEE Transactions on Pattern Analysis and Machine Intelligence*, 35(6), 1397-1409, doi: 10.1109/TPAMI.2012.213

15. Zhu, Y., Tang, G., Zhang, X., Jiang, J., and Tian, Q. (2017). Haze removal method for natural restoration of images with Sky, *Neurocomputing*, 275, 499-510, doi: 10.1016/j.neucom.2017.08.055

16. Yuan, H., Liu, C., Guo, Z., and Sun, Z. (2017). A region-wised medium transmission based image dehazing method, *IEEE Access*, 5, 1735-1742, doi: 10.1109/ACCESS.2017.2660302

17. Wang, W., Yuan, X., Wu, X., and Liu, Y. (2017). Dehazing for images with large sky region, *Neurocomputing*, 238, 365-376, doi: 10.1016/j.neucom.2017.01.075

18. Zhu, M., He, B., and Wu, Q. (2018). Single image dehazing based on dark channel prior and energy minimization, *IEEE Signal Processing Letters*, 25(2), 174-178, doi: 10.1109/LSP.2017.2780886

19. Xiao, J., Zhu, L., Zhang, Y., Liu, E., and Lei, J. (2017). Scene-aware image dehazing based on sky-segmented dark channel prior, *IET Image Processing*, 11(12), 1163-1171, doi: 10.1049/iet-ipr.2017.0058

20. Liu Q. (2018). A light intensity reverse algorithm for improving dark channel prior dehazing, *Proc. of the 11th International Congress on Image and Signal Processing, BioMedical Engineering and Informatics*, Beijing, China, 1-9, doi: 10.1109/CISP-BMEI.2018.8633085

21. Chen, Y., Li, Z., Bhanu, B., Tang, D., Peng, Q., et. al. (2018). Improve transmission by designing filters for image dehazing, *Proc. of IEEE the 3rd International Conference on Image, Vision and Computing*, Chongqing, China, 374-378, doi: 10.1109/ICIVC.2018.8492834

22. Zhang, L., Wang, S., and Wang, X. (2018). Saliency-based dark channel prior model for single image haze removal, *IET Image Processing*, 12(6), 1049-1055, doi: 10.1049/iet-ipr.2017.0959

23. Salazar-Colores, S., Cabal-Yepez, E., Ramos-Arreguin, J.M., Botella, G., Ledesma-Carrillo, L.M., et. al. (2019). A fast image dehazing algorithm using morphological reconstruction, *IEEE Transactions on Image Processing*, 28(5), 2357-2366, doi: 10.1109/TIP.2018.2885490

24. Putra, O.V., Musthafa, A., and Pradhana, F. R. (2019). 'A hybrid approach on single image dehazing using adaptive gamma correction, *J. Phys.: Conf. Ser.* 1381 012030, doi: 10.1088/1742-6596/1381/1/012030

25. Ju, M., Ding, C., Zhang, D., and Guo, Y.J. (2018). Gamma-correction-based visibility restoration for single hazy images, *IEEE Signal Processing Letters*, 25(7), 1084-1088, doi: 10.1109/LSP.2018.2839580

26. Kapoor, R., Gupta, R., Son, L.H., Kumar, R., and Jha, S. (2019). Fog removal in images using improved dark channel prior and contrast limited adaptive histogram equalization, *Multimedia Tools and Applications*, 78, 23281-23307, doi: 10.1007/s11042-019-7574-8

27. Shen, Y., Wu, X., and Deng, X. (2015). Analysis on spectral effects of dark-channel prior for haze removal, *Proc. of IEEE International Conference on Image Processing*, Quebec City, QC, 2945-2949, doi: 10.1109/ICIP.2015.7351342

28. Ma, K., Liu, W., and Wang, Z. (2015). Perceptual evaluation of single image dehazing algorithms, *Proc. of IEEE International Conference on Image Processing*, Quebec City, QC, 3600-3604, doi: 10.1109/ICIP.2015.7351475

29. Indoor training set, Available https://www.dropbox.com/sh/mrtguzk1a1l11o6/AAArCkAhSQ-LZ34psGM5MuUZa?dl=0.

30. Outdoor training set, Available https://www.dropbox.com/s/86qp410gen5u2uk/ITS.zip?dl=0.

31. Shin, J., Kim, M., Paik, J., and Lee, S. (2020). Radiance–reflectance combined optimization and structure-guided l_0-norm for single image dehazing, *IEEE Transactions on Multimedia*, 22(1), 30-44, doi: 10.1109/TMM.2019.2922127

32. Zhu, Q., Mai, J., and Shao, L. (2015). A fast single image haze removal algorithm using color attenuation prior, *IEEE Transactions on Image Processing*, 24(11), 3522-3533, doi: 10.1109/TIP.2015.2446191

33. Cai, B., Xu, X., Jia, K., Qing, C., and Tao, D. (2016). DehazeNet: an end-to-end system for single image haze removal, *IEEE Transactions on Image Processing*, 25(11), 5187-5198, doi: 10.1109/TIP.2016.2598681

34. Wang, Z., Bovik, A.C., Sheikh, H.R., and Simoncelli, E. P. (2004). Image quality assessment: from error visibility to structural similarity, *IEEE Transactions on Image Processing*, 13(4), 600-612, doi: 10.1109/TIP.2003.819861

35. Min, X., Zhai, G., Gu, K., Yang, X., and Guan, X. (2019). Objective quality evaluation of dehazed images, *IEEE Transactions on Intelligent Transportation Systems*, 20(8), 2879-2892, doi: 10.1109/TITS.2018.2868771

36. Mittal, A., Moorthy, A.K., and Bovik, A.C. (2012). "No-reference image quality assessment in the spatial domain, *IEEE Transactions on Image Processing*, 21(12), 4695-4708, doi: 10.1109/TIP.2012.2214050

37. Zhang, L., Zhang, L., and Bovik, A.C. (2015). A feature-enriched completely blind image quality evaluator, *IEEE Transactions on Image Processing*, 24(8), 2579-2591, doi: 10.1109/TIP.2015.2426416